E-ISSN: 2829-7687
Journal of Fibers and Polymer Composites
Vol. 5 No. 2 (2026): 117-134

Hybrid Natural-Synthetic Fiber Composites for Noise and Vibration Control: Linking Acoustic Performance to Environmental Sustainability Metrics

Fauzi Ibrahim [a] *, Rani Ismiarti Ergantara [b], Ambar Pambudi [c]

[a] Department of Automotive Engineering Technology, Politeknik Negeri Lampung, Lampung, Indonesia
[b] Environmental Engineering, Universitas Malahayati, Lampung, Indonesia
[c] Department Agricultural Mechanization, Politeknik Negeri Lampung, Lampung, Indonesia

Abstract. *Hybrid natural-synthetic fiber composites are attractive for automotive acoustic trim only when composition effects are separated from geometric effects and the computational assumptions are fully reproducible. This study presents a transparent screening framework linking normal-incidence acoustic absorption, a literature-informed vibration-damping proxy, specific stiffness, mass and constituent-production environmental metrics. Twelve polypropylene-based formulations were compared at a common thickness of 20 mm; 16, 20 and 24 mm were then evaluated separately in the thickness-sensitivity analysis. Open porosity and flow resistivity were generated by explicit bounded composition-to-property rules and used in the Miki equivalent-fluid model. Environmental inputs were evaluated with 20,000-trial triangular uncertainty propagation, while the multi-criteria ranking used winsorized normalization and 10,000 weight-perturbation scenarios of +/-15%. At 20 mm, broadband absorption averages (500-4000 Hz) occupied a narrow range of 0.612-0.636, demonstrating that acoustic comparisons are sensitive to geometry and that thickness must be controlled when isolating composition effects. Increasing thickness from 16 to 24 mm raised the modeled broadband absorption of representative natural-fiber-rich panels from about 0.55 to 0.69. C25-G10-R5 ranked first under the baseline weights and in 100% of weight-perturbation scenarios; JC30-G10 remained in the top three in 100% of scenarios and C35-rP5 in 79.1%. Median constituent-production greenhouse-gas reductions relative to GF40-PP ranged from approximately 26% to 56% for the non-aramid hybrid candidates, whereas the aramid-containing design was environmentally unfavorable. The reported damping values are screening proxies, not measured loss factors, and the environmental calculation is not a full ISO-compliant comparative LCA. The framework is therefore intended for hypothesis generation and experimental down-selection rather than direct certification of material performance.*

Keywords: *hybrid composites; natural fibers; acoustic absorption; vibration damping; environmental screening; automotive trim.*

1. Introduction

Automotive interior noise and vibration control is increasingly coupled with mass reduction, circular-material strategies and embodied-impact targets [1−9]. Glass-fiber-reinforced thermoplastics provide stiffness and dimensional stability, but natural fibers such as jute, flax, kenaf, hemp and coir offer lower density, renewable feedstocks and porous multiscale structures that can dissipate acoustic energy [10−14]. Their limitations include moisture sensitivity, property

https://doi.org/10.55043/jfpc.v5i2.692
Received July 1, 2026; Received in revised July 9, 2026; Accepted July 11, 2026; Published July 27, 2026
* Corresponding author
Email: fauziibrahim@polinela.ac.id

variability and reduced stiffness margins, which motivates hybridization with glass, basalt, recycled polymer fibers or localized elastomeric phases [15−24].

Recent experimental and applied studies have examined acoustic and vibration behavior more directly. Senthilrajan et al. quantified mechanical, damping and acoustic responses of jute/aloe-vera hybrid laminates [25]. Work on enset woven structures [26] and natural-fiber micro-perforated/fibrogranule absorbers [27] further demonstrates that architecture, backing configuration and porous morphology strongly influence sound absorption. Nikhil et al. reported the sensitivity of vibration response and damping to coir-fiber content [28], while Tengku et al. investigated dynamic stiffness and damping in treated natural-fiber/fiberglass hybrids [29]. Astrauskas et al. showed that absorber thickness strongly affected acoustic performance and that changing hemp-shive content altered porosity and airflow resistivity in rubber-based composites [30]. Shen et al. measured the acoustic response of jute/polypropylene composites using an impedance-tube approach [31], and Pingulkar et al. demonstrated that glass-fiber hybridization modifies the dynamic response of jute- and flax-based laminates [32]. These studies reinforce two methodological requirements for a computational screen: geometry must not be confounded with composition, and porous-acoustic and damping inputs must be reported explicitly.

Related pre-screening and hybrid-design studies have also examined green-material noise-reduction concepts [33], natural/synthetic hybrid property balance [34], and the effect of interply versus intraply jute-glass architecture on mechanical performance [35]. Three gaps therefore motivate the present work. First, acoustic, vibration-related and environmental metrics are commonly reported separately, which complicates early-stage material down-selection. Second, computational screening studies can become irreproducible when porosity, airflow resistivity or damping assignments are hidden. Third, multi-criteria rankings may be artifacts of a single weight set or extreme normalization values. The present framework addresses these issues by comparing all formulations at 20 mm, publishing all composition-to-property equations, propagating uncertainty in greenhouse-gas factors and perturbing all MCDA weights by +/-15%.

The novelty is the integration of a transparent acoustic-vibration-stiffness (AVS) screening index with uncertainty-aware environmental screening and ranking robustness. The study does not claim fabricated specimens or measured properties. Harshness is also not modeled as a direct psychoacoustic quantity; specific stiffness is used only as a structural-response proxy and must not be interpreted as a direct measure of perceived harshness. The acoustic screen uses the Miki equivalent-fluid formulation [36], and the computational outputs are intended to define testable hypotheses for subsequent impedance-tube testing under ISO 10534-2:2023 or ASTM E1050-24 and damping validation under ASTM E756-05(2023) [37−39].

2. Materials and methods

2.1. Research design and functional unit

A virtual design-of-experiments was established for automotive interior acoustic trim panels. The primary functional unit was 1 m² of panel with a nominal thickness of 20 mm. Holding thickness constant removes a major geometric confound and makes the composition comparison internally consistent. Thickness was then evaluated separately at 16, 20 and 24 mm for five representative formulations. Thus, the primary ranking answers a material-composition question under a common 20 mm geometry, while the sensitivity analysis quantifies the independent geometric effect.

No physical specimens were fabricated or tested. The model uses explicit screening rules for open porosity and airflow resistivity, the Miki equivalent-fluid formulation for a rigidly backed porous layer, a disclosed literature-informed damping proxy, a micromechanics-inspired specific-modulus proxy, and constituent-production environmental factors. These outputs are deterministic or uncertainty-propagated model results; none should be represented as measured experimental data.

Table 1. Virtual design variables and controls for the computational study

Design variable	Level or definition	Engineering purpose
Natural fiber type	Jute, flax, kenaf, hemp, coir	Renewable reinforcement and pore-forming phase
Synthetic phase	E-glass, basalt, recycled PET, aramid	Stiffness retention, durability or recycled content
Elastomeric filler	Waste-tire rubber, 0-5 wt%	Damping-oriented screening term and impedance tuning
Matrix	Polypropylene + 3 wt% MAPP unless formulation balance requires otherwise	Automotive thermoplastic baseline
Primary thickness	20 mm for all 12 formulations	Fair composition comparison
Thickness sensitivity	16, 20 and 24 mm	Independent geometric effect
Acoustic inputs	Open porosity φ and airflow resistivity σ	Reproducible Miki-model inputs
Acoustic metric	α(f), BAA and NRC proxy	Normal-incidence absorption indicators
AVS metric	BAA, η and specific modulus proxy	Acoustic-vibration-stiffness screening
Environmental metric	GHG, CED, areal mass, renewable/recycled share	Constituent-production screening, not full comparative LCA
Robustness analysis	20,000 environmental draws; 10,000 weight scenarios	Uncertainty and ranking stability

2.2. Composite formulation matrix

The formulation mass fractions are listed in Table 2, and all formulations are compared at 20 mm in the primary analysis. GF40-PP and JC40-PP are boundary benchmarks; the remaining entries are true hybrid candidates.

2.3. Constituent properties, environmental factors and uncertainty

Table 3 lists the central screening values. Units are reported in parentheses as requested. PP and glass-fiber factors were anchored to published industry LCA datasets [40,41], recycled-plastic direction and uncertainty were informed by the APR/Franklin comparison [42], and natural-fiber uncertainty was broadened because cultivation, allocation and processing assumptions strongly affect reported impacts [43]. The remaining factors are literature-calibrated engineering screening values and are not presented as a database-quality inventory.

Table 2. Formulation matrix of benchmark and hybrid composite panels

Code	Natural fibers (wt%)	Synthetic fibers/fillers (wt%)	Matrix system (wt%)	Purpose
GF40-PP	-	glass 40	PP 57 + MAPP 3	Synthetic glass benchmark
J30-G10	jute 30	glass 10	PP 57 + MAPP 3	Jute/glass balanced hybrid
F25-G15	flax 25	glass 15	PP 57 + MAPP 3	Flax/glass stiffness-oriented hybrid
K30-rP10	kenaf 30	rPET 10	PP 57 + MAPP 3	Kenaf/recycled-PET route
C25-G10-R5	coir 25	glass 10; rubber 5	PP 57 + MAPP 3	Coir/glass/rubber damping-oriented hybrid
H25-B15	hemp 25	basalt 15	PP 57 + MAPP 3	Hemp/basalt stiffness-oriented hybrid
J20-A10-R5	jute 20	aramid 10; rubber 5	PP 62 + MAPP 3	Local impact/damping concept
F35-rP5	flax 35	rPET 5	PP 57 + MAPP 3	Flax/recycled-PET acoustic concept
K25-G15-R3	kenaf 25	glass 15; rubber 3	PP 54 + MAPP 3	Balanced kenaf/glass/rubber hybrid
C35-rP5	coir 35	rPET 5	PP 57 + MAPP 3	Coir/recycled-PET low-carbon concept
JC30-G10	jute 15; coir 15	glass 10	PP 57 + MAPP 3	Jute-coir/glass broadband concept
JC40-PP	jute 20; coir 20	-	PP 57 + MAPP 3	Natural-fiber boundary benchmark

Table 3. Central constituent-property values used in the screening model

Constituent	Family	Density (kg m^{-3})	E (GPa)	GHG (kg CO_2e kg^{-1})	CED (MJ kg^{-1})	Renewable (%)	Recycled (%)
PP	Matrix	900	1.40	1.95	75.5	0	0
MAPP	Compatibilizer	920	1.20	2.50	85	0	0
jute	Natural fiber	1450	30.0	0.60	12	100	0
flax	Natural fiber	1500	50.0	0.75	20	100	0
kenaf	Natural fiber	1400	35.0	0.65	15	100	0
hemp	Natural fiber	1480	35.0	0.70	18	100	0
coir	Natural fiber	1150	6.0	0.45	10	100	0
glass	Synthetic fiber	2550	72.0	1.44	39	0	0
basalt	Mineral fiber	2700	88.0	2.30	65	0	0
rPET	Recycled synthetic fiber	1380	5.0	0.90	30	0	100
aramid	Synthetic fiber	1440	70.0	20.0	200	0	0
rubber	Recycled elastomer filler	1100	0.05	0.25	8	0	100

For greenhouse-gas uncertainty, each central factor g_i was sampled from a triangular distribution with lower and upper bounds $g_i(1-u_i)$ and $g_i(1+u_i)$. Relative half-ranges u_i were 20% for PP and glass, 30% for MAPP, 35% for basalt and rPET, 40% for aramid, and 50% for natural fibers and recycled rubber. Twenty thousand Monte Carlo trials were performed with a fixed random seed. This uncertainty analysis addresses input sensitivity but does not convert the calculation into a full ISO 14040/14044 comparative LCA.

2.4. Acoustic, damping and stiffness modeling

Open porosity and airflow resistivity are defined explicitly. Let N denote total natural-fiber content in percentage points and let rPET, R, G, B and A denote the wt% of recycled PET, rubber, glass, basalt and aramid, respectively. The composition-to-porosity and composition-to-flow-resistivity screening equations are given as native equations in Table 4. These mappings are transparent hypotheses rather than measured material laws; future experimental work should replace them with measured porosity and airflow resistivity.

Table 4. Equations, coefficients and selection metrics used in the computational framework

Metric	Expression	Interpretation
Solid mixture density	$\rho_s = \left(\sum_i \frac{w_i}{\rho_i}\right)^{-1}$	Mass-fraction inverse mixture rule
Open porosity	$\phi = \mathrm{clip}(0.18 + 0.007N + 0.003\,\mathrm{rPET} + 0.004R$ $-0.002G - 0.002B - 0.001A,\ 0.18,\ 0.55)$	Explicit composition-to-porosity screening rule
Bulk density	$\rho_b = (1-\phi)\rho_s$	Porosity-adjusted apparent density
Flow resistivity	$\sigma = \mathrm{clip}(100000 - 1200N - 600\,\mathrm{rPET} - 400R$ $+500G + 700B + 400A,\ 50000,\ 250000)$	Explicit model input, Pa s m⁻²
Miki impedance	$\frac{Z_c}{\rho_0 c_0} = 1 + 0.070\left(\frac{f}{\sigma}\right)^{-0.632}$ $-j\,0.107\left(\frac{f}{\sigma}\right)^{-0.632}$	Equivalent-fluid characteristic impedance [36]
Miki propagation	$\gamma = \frac{\omega}{c_0}\{0.160\left(\frac{f}{\sigma}\right)^{-0.618}$ $+j\left[1 + 0.109\left(\frac{f}{\sigma}\right)^{-0.618}\right]\}$	Complex propagation constant [36]
Rigid-backed surface impedance	$Z_s = Z_c \coth(\gamma d)$	Layer of thickness d
Absorption coefficient	$\alpha = 1 - \left\lvert\frac{Z_s - \rho_0 c_0}{Z_s + \rho_0 c_0}\right\rvert^2$	Normal incidence
BAA	$\mathrm{BAA} = \frac{\alpha_{500} + \alpha_{1000} + \alpha_{2000} + \alpha_{4000}}{4}$	Study-specific broadband indicator
Damping proxy	$\hat{\eta} = \sum_i w_i c_i + 0.006 I_{ns}$ $+0.004\frac{\phi - 0.18}{0.37}$ $I_{ns} = \frac{4 w_n w_s}{(w_n + w_s)^2}$	Hybrid interaction term; active only when both natural and synthetic phases are present.
Specific modulus proxy	$E_{\mathrm{eff}} = \left(\sum_i V_i \kappa_i E_i\right)(1-\phi)^2$ $\mathrm{SpecE} = \frac{E_{\mathrm{eff}}}{\rho_b/1000}$	Architecture-efficiency proxy; κ disclosed in text
Environmental inventory	$\mathrm{GHG}_A = m_A \sum_i w_i g_i$ $\mathrm{CED}_A = m_A \sum_i w_i e_i$	Constituent-production screening per m²
Robust normalization	$x_n = \mathrm{clip}\left(\frac{x - Q_{10}}{Q_{90} - Q_{10}},\ 0,\ 1\right)$	10th-90th percentile winsorized min-max
AVS index	$\mathrm{AVS} = 0.55\,\mathrm{BAA}_n + 0.30\,\hat{\eta}_n + 0.15\,\mathrm{SpecE}_n$	Acoustic-vibration-stiffness performance
Sustainability index	$S = 0.45\,\mathrm{lowGHG}_n + 0.30\,\mathrm{lowCED}_n$ $+0.15\,\mathrm{lowMass}_n + 0.10\,\mathrm{Renewable}_n$	Screening index
MCDA score	$\mathrm{MCDA} = 100(0.60\,\mathrm{AVS} + 0.40S)$	Baseline ranking; all weights perturbed by ±15%

The acoustic layer was modeled with the Miki modification of the Delany-Bazley empirical model [36]. For frequency f, ambient density ρ_0 and sound speed c_0, the characteristic impedance and propagation constant were calculated from the equations in Table 4. The rigid-backed surface impedance was then used to obtain the normal-incidence absorption coefficient. The model is intended for high-porosity fibrous absorbers and may not represent a highly consolidated compression-molded PP composite. Therefore, the predicted spectra are treated as comparative screening outputs and are externally sanity-checked against measured literature trends rather than claimed as validated material properties.

Broadband Absorption Average (BAA) is defined here as the mean of α at 500, 1000, 2000 and 4000 Hz. It provides a compact study-specific indicator of broadband absorption over frequencies relevant to interior airborne-noise control; it is not a standardized certification metric. The NRC proxy is the mean at 250, 500, 1000 and 2000 Hz and is reported only as a screening analogue.

The vibration quantity $\hat{\eta}$ is deliberately renamed a damping screening proxy. It is not a measured material loss factor. Constituent coefficients c_i were assigned as follows: PP 0.010, MAPP 0.012, jute 0.035, flax 0.032, kenaf 0.034, hemp 0.036, coir 0.050, glass 0.006, basalt 0.006, rPET 0.025, aramid 0.020 and rubber 0.120. These directional choices are consistent with recent experimental damping studies [25,28,29,32], but the resulting proxy cannot independently prove that a constituent increases damping because that tendency is partly encoded in the coefficients. Accordingly, damping-related conclusions are framed as scenario outcomes to be validated under ASTM E756-05(2023) [39].

For the specific-modulus proxy, constituent volume fractions V_i were calculated from composition and density. Architecture-efficiency factors κ_i were 1.0 for PP/MAPP, 0.12 for natural fibers, 0.22 for glass/basalt/aramid, 0.15 for rPET and 0.05 for rubber. These factors represent an early-stage discontinuous/partially aligned trim architecture and are not substitutes for tensile or flexural measurements.

2.5. Environmental screening and multi-criteria robustness

The environmental calculation is framed as constituent-production environmental screening rather than an ISO-compliant comparative LCA. The primary system boundary includes only the embodied GHG and CED factors assigned to the constituent masses in a 1 m^2 × 20 mm panel. Panel-forming energy is not included because process-specific data are not available. Transport, molding electricity, use phase, acoustic system-level benefits, service life and end-of-life credits are outside the boundary. Consequently, the results support relative hypothesis generation only.

The primary MCDA used the baseline weights shown in Table 4. No claim is made that these weights represent a universal preference structure. To reduce outlier distortion, each normalized criterion used 10th-90th percentile winsorized min-max scaling. Ranking robustness was then evaluated in 10,000 scenarios in which every performance, sustainability and group-level weight was independently multiplied by a uniform factor between 0.85 and 1.15 and renormalized within its group. Top-1 and top-3 frequencies are reported.

3. Results and discussion

3.1. Physical and model-input space

Table 5 reports the 20 mm results and makes φ and σ explicit. Because the same 20 mm geometry is used for all formulations, areal mass varies with composition and the assigned open porosity. GF40-PP remains the densest option at 19.93 kg m^{-2}, whereas C35-rP5 and JC40-PP are close to 11.1 kg m^{-2}. The explicit σ values span 52-120 kPa s m^{-2}, and φ spans 0.18-0.46.

At 20 mm, BAA values span only 0.612-0.636. This narrow range shows that composition alone produces modest separation in broadband absorption under equal geometry. Composition still modifies the shape of the modeled spectrum through σ, but thickness remains a major independent driver and must be controlled before comparing materials.

Table 5. Model inputs and outputs for all formulations

Code	ρ (kg m^{-3})	φ (-)	σ (kPa s m^{-2})	mA (kg m^{-2})	BAA (-)	$\hat{\eta}$ (-)	Spec. E	GHG (kg CO_2e m^{-2})	CED (MJ m^{-2})
GF40-PP	997	0.180	120.0	19.93	0.612	0.0085	2.80	35.13	1220
J30-G10	691	0.370	69.0	13.81	0.636	0.0237	1.44	20.87	733
F25-G15	757	0.325	77.5	15.14	0.635	0.0222	1.93	24.08	855
K30-rP10	609	0.420	58.0	12.18	0.634	0.0259	1.09	17.92	646
C25-G10-R5	666	0.355	73.0	13.33	0.636	0.0319	1.10	19.40	698
H25-B15	758	0.325	80.5	15.16	0.634	0.0232	1.83	25.87	907
J20-A10-R5	688	0.330	78.0	13.75	0.635	0.0285	1.72	46.99	992
F35-rP5	599	0.440	55.0	11.97	0.632	0.0239	1.32	17.89	648
K25-G15-R3	739	0.337	76.3	14.78	0.635	0.0261	1.70	22.37	786
C35-rP5	556	0.440	55.0	11.13	0.632	0.0302	0.66	15.46	563
JC30-G10	671	0.370	69.0	13.42	0.636	0.0260	1.27	19.97	708
JC40-PP	552	0.460	52.0	11.05	0.630	0.0261	0.84	15.42	552

BAA denotes the average absorption coefficient over 500-4000 Hz. The damping quantity is a disclosed screening proxy rather than a measured loss factor. GHG and CED refer to constituent production for the 1 m² × 20 mm functional unit.

3.2. Acoustic spectra and thickness sensitivity

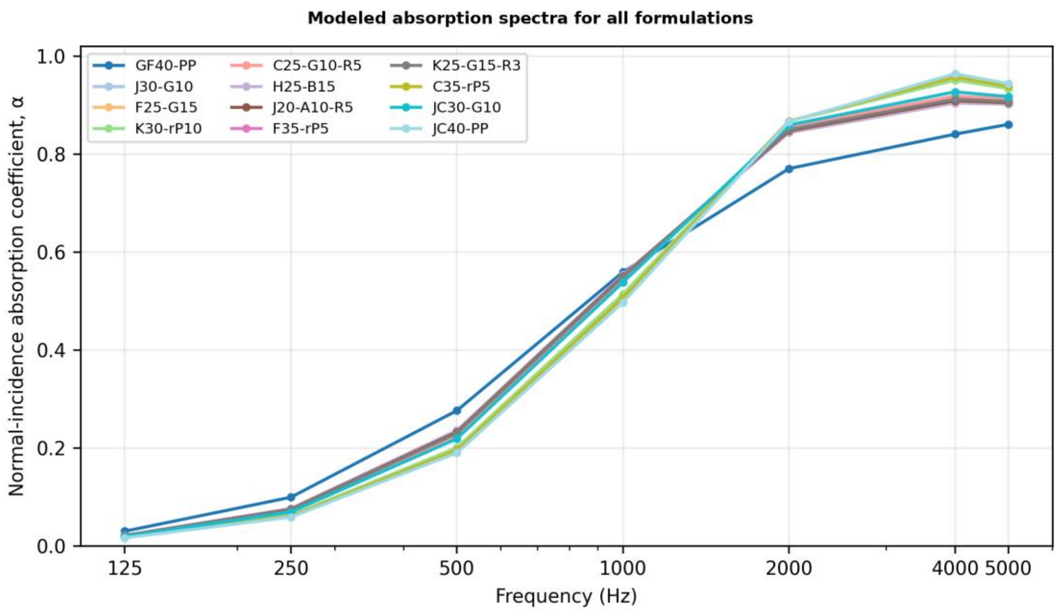

Fig. 1. Modeled normal-incidence absorption spectra for all formulations

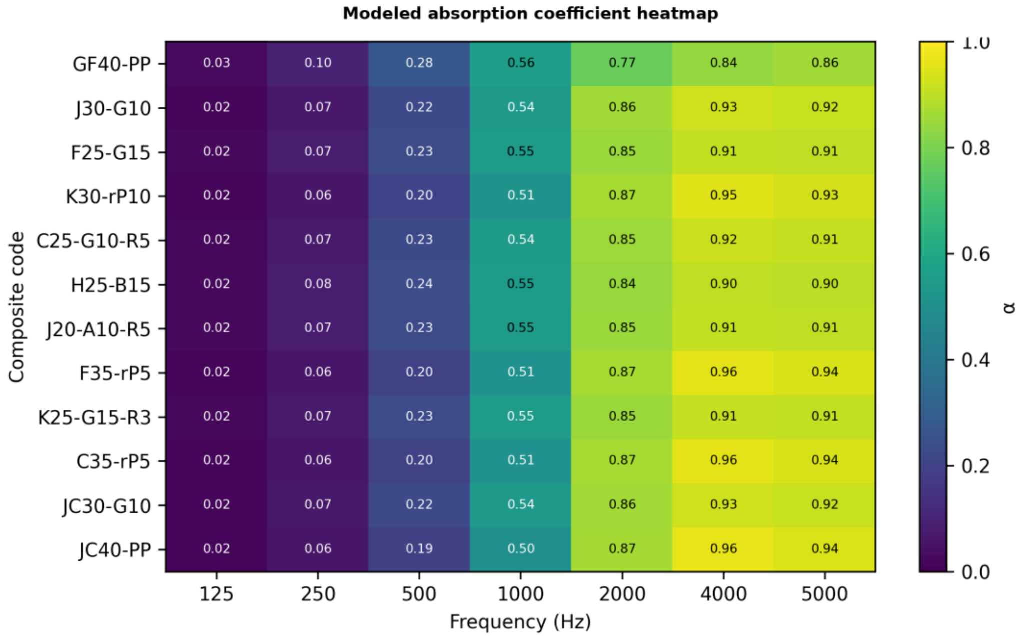

Fig. 2. Heatmap of modeled absorption coefficients at octave-like frequencies

At 20 mm, the spectra are closely clustered. The glass benchmark has slightly higher modeled absorption at 125-500 Hz because its larger assigned σ shifts the impedance relation, whereas several natural-fiber-rich formulations become stronger above 1000 Hz. The maximum values remain below 0.99; the 4000 Hz values range from 0.84 to 0.96. This conservative result is consistent with treating the model as a screen rather than a substitute for impedance-tube measurements [25,30,31].

Table 6. Frequency-dependent modeled absorption coefficients

Code	125 Hz	250 Hz	500 Hz	1000 Hz	2000 Hz	4000 Hz	5000 Hz
GF40-PP	0.03	0.10	0.28	0.56	0.77	0.84	0.86
J30-G10	0.02	0.07	0.22	0.54	0.86	0.93	0.92
F25-G15	0.02	0.07	0.23	0.55	0.85	0.91	0.91
K30-rP10	0.02	0.06	0.20	0.51	0.87	0.95	0.93
C25-G10-R5	0.02	0.07	0.23	0.54	0.85	0.92	0.91
H25-B15	0.02	0.08	0.24	0.55	0.84	0.90	0.90
J20-A10-R5	0.02	0.07	0.23	0.55	0.85	0.91	0.91
F35-rP5	0.02	0.06	0.20	0.51	0.87	0.96	0.94
K25-G15-R3	0.02	0.07	0.23	0.55	0.85	0.91	0.91
C35-rP5	0.02	0.06	0.20	0.51	0.87	0.96	0.94
JC30-G10	0.02	0.07	0.22	0.54	0.86	0.93	0.92
JC40-PP	0.02	0.06	0.19	0.50	0.87	0.96	0.94

All values are model outputs at 20 mm, not impedance-tube measurements. Experimental validation should follow ISO 10534-2:2023 or ASTM E1050-24 [37,38].

The thickness-sensitivity analysis isolates the geometry effect. For C35-rP5 and F35-rP5, BAA increases from 0.550 at 16 mm to 0.687 at 24 mm; JC30-G10 increases from 0.564 to 0.683. The GF40-PP benchmark also increases, from 0.567 to 0.637. Therefore, comparisons between a 24 mm hybrid and a 16 mm glass benchmark cannot isolate composition effects. Accordingly, the main material ranking is based on the 20 mm dataset.

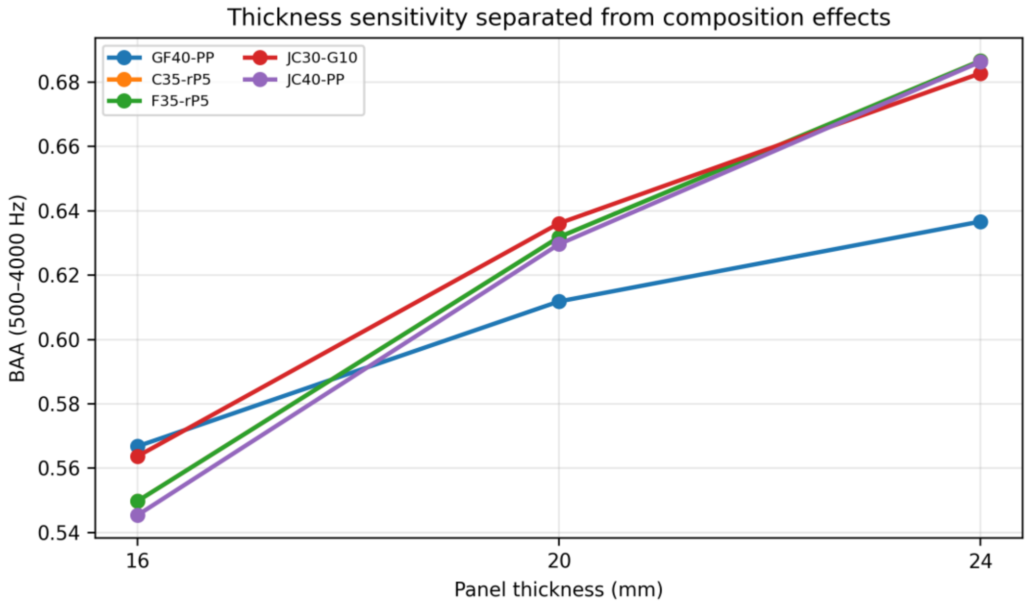

Fig. 3. Independent thickness sensitivity for representative formulations

3.3. Damping-proxy and specific-stiffness trade-off

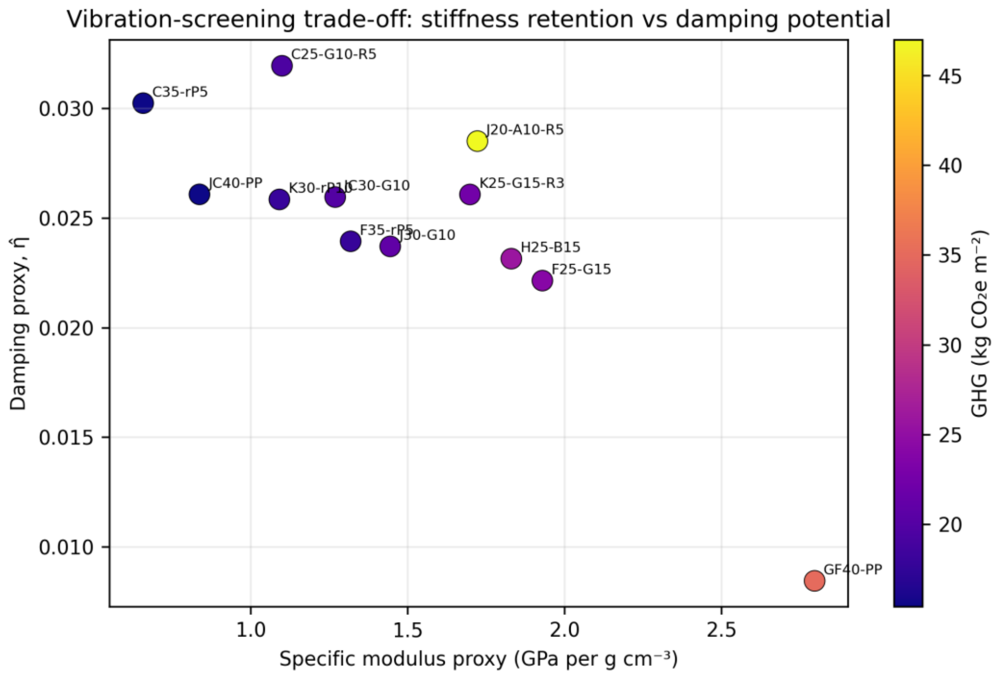

Fig. 4. Screening map of disclosed damping proxy versus specific-stiffness proxy

The screening map should be interpreted as a consequence of the stated proxy equations. GF40-PP has the highest specific-modulus proxy and the lowest $\hat{\eta}$. C25-G10-R5 and C35-rP5 move toward higher $\hat{\eta}$ because the disclosed coefficient set assigns larger damping contributions to rubber, coir and porosity. This result is useful for scenario ranking, but it is not independent evidence that these constituents increase measured damping. Experimental literature supports the direction of the hypothesis [25,28,29], and ASTM E756-type testing is required to determine actual loss factors [39].

This formulation avoids a circular interpretation. The model asks which candidates would be favored under an explicit, literature-informed damping scenario, not whether the model has experimentally discovered the damping mechanism.

3.4. Environmental screening with input uncertainty

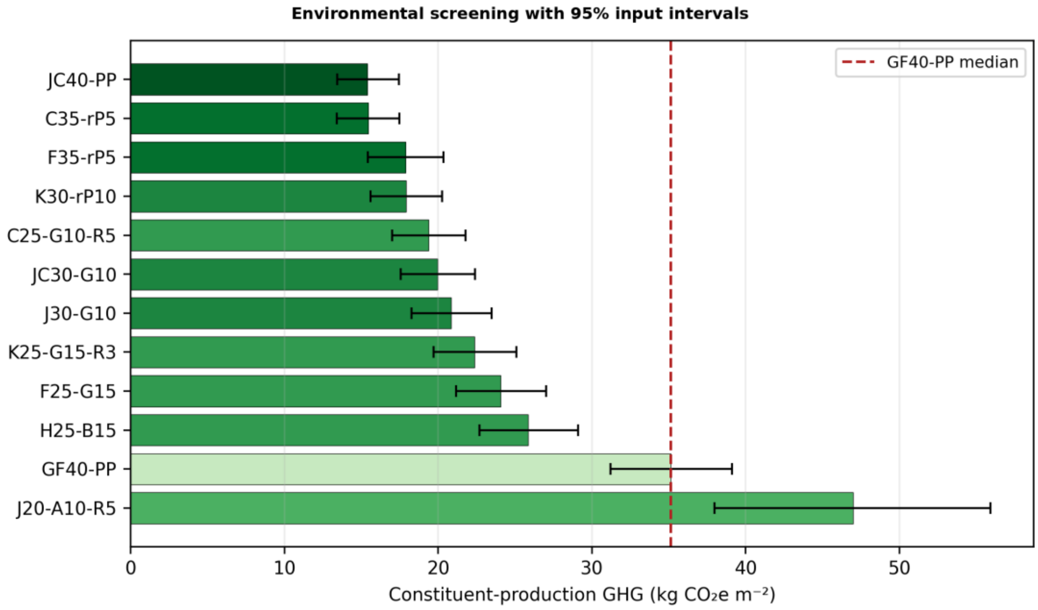

Fig. 5. Constituent-production GHG medians and 95% uncertainty intervals for the composite panels

Table 7. Environmental screening results relative to the GF40-PP benchmark

Code	GHG median (kg CO_2e m^{-2})	95% interval	GHG reduction median % (95% interval)	Renew. wt%	Recycl. wt%
GF40-PP	35.12	31.20-39.12	Baseline	0	0
J30-G10	20.85	18.27-23.48	40.6 (36.9 to 44.3)	30	0
F25-G15	24.07	21.16-27.01	31.5 (27.5 to 35.3)	25	0
K30-rP10	17.90	15.59-20.26	49.0 (45.0 to 53.0)	30	10
C25-G10-R5	19.38	17.01-21.78	44.8 (42.0 to 47.7)	25	5
H25-B15	25.86	22.68-29.11	26.4 (19.7 to 32.6)	25	0
J20-A10-R5	46.99	37.98-55.92	-33.6 (-61.1 to -8.5)	20	5
F35-rP5	17.88	15.43-20.34	49.1 (44.5 to 53.5)	35	5
K25-G15-R3	22.37	19.71-25.08	36.3 (32.9 to 39.6)	25	3
C35-rP5	15.45	13.41-17.49	56.0 (52.8 to 59.3)	35	5
JC30-G10	19.95	17.57-22.38	43.2 (40.3 to 46.1)	30	0
JC40-PP	15.41	13.43-17.43	56.1 (52.9 to 59.3)	40	0

Table 7 summarizes the uncertainty information required to interpret the headline environmental result. GF40-PP has a median of 35.12 kg CO_2e m^{-2} (95% interval 31.20-39.12). Among the non-aramid hybrid candidates, median reductions range from 26.4% for H25-B15 to 56.0% for C35-rP5. In the Monte Carlo screening, all of these candidates remain below the GF40-PP baseline in essentially 100% of trials. The aramid-containing J20-A10-R5 behaves differently: its median burden is 46.99 kg CO_2e m^{-2} and its median change is 33.6% worse than the glass benchmark.

These ranges do not establish a comparative LCA result because transport, molding, regional electricity, use phase and end of life are excluded. They show only that the direction of the constituent-production comparison is robust to the stated factor uncertainty for most candidates.

The aramid case also illustrates why a technically attractive reinforcement cannot be assumed to be environmentally preferable.

3.5. Linking AVS performance to environmental screening

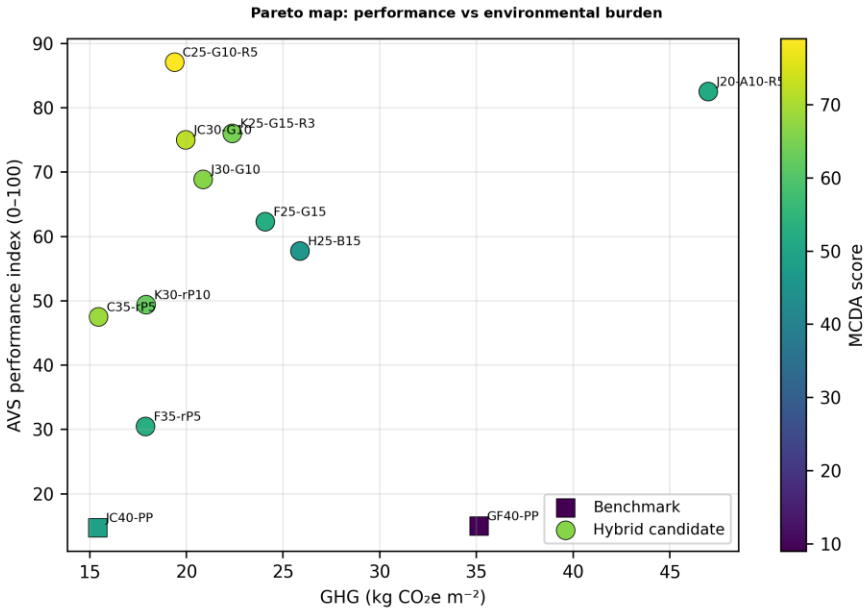

Fig. 6. Pareto map linking the AVS performance index to constituent-production GHG burden

Table 8. Multi-criteria ranking and top-three stability under +/-15% weight perturbation

Rank	Code	Class	AVS	Sust.	MCDA	Top-3 freq. (%)	Engineering interpretation
1	C25-G10-R5	Hybrid candidate	87.1	66.9	79.0	100.0	Highest overall score; damping-oriented true hybrid under stated proxy assumptions.
2	JC30-G10	Hybrid candidate	75.0	67.8	72.1	100.0	Balanced acoustic, stiffness and environmental profile; top-three stable.
3	C35-rP5	Hybrid candidate	47.5	100.0	68.5	79.1	Lowest-carbon true hybrid cluster; top-three robust in most weight scenarios.
4	J30-G10	Hybrid candidate	68.9	62.3	66.2	20.3	Conservative glass-containing option; top-three in some weight scenarios.
5	K25-G15-R3	Hybrid candidate	76.0	47.7	64.7	0.6	Moderate damping/stiffness balance; low top-three frequency.
6	K30-rP10	Hybrid candidate	49.4	82.0	62.5	0.0	Low-impact recycled-synthetic route; moderate AVS performance.
7	F35-rP5	Hybrid candidate	30.5	86.2	52.8	0.0	Low GHG and mass, but lower normalized damping/stiffness balance.
8	F25-G15	Hybrid candidate	62.3	37.2	52.2	0.0	High stiffness proxy with higher mass and environmental burden.
9	J20-A10-R5	Hybrid candidate	82.5	5.3	51.7	0.0	Technical proxy performance offset by aramid environmental burden.
10	JC40-PP	Benchmark	14.7	100.0	48.8	0.0	Boundary benchmark; low burden but weak stiffness proxy.
11	H25-B15	Hybrid candidate	57.7	28.9	46.2	0.0	Stiffness-oriented route with higher mineral-fiber burden.
12	GF40-PP	Benchmark	15.0	0.0	9.0	0.0	High specific stiffness; poorest combined environmental/AVS score.

Table 8 tests whether the engineering ranking remains stable under weight uncertainty.

Under the baseline weights, C25-G10-R5 ranks first with an MCDA score of 79.0, followed by JC30-G10 (72.1) and C35-rP5 (68.5). More importantly, C25-G10-R5 is rank 1 in 100% of the 10,000 perturbed-weight scenarios, JC30-G10 remains in the top three in 100%, and C35-rP5 remains in the top three in 79.1%. J30-G10 enters the top three in 20.3% of scenarios. The top candidate is therefore not a single-weight artifact within the tested +/-15% range.

Under the disclosed framework, C25-G10-R5 ranks first because the analysis combines a common 20 mm geometry, winsorized normalization, environmental uncertainty and an explicit damping proxy. This result illustrates that computational rankings are conditional on model definition; therefore, candidate selection should be interpreted together with the sensitivity and uncertainty analyses rather than as an absolute material hierarchy.

Table 9. Correlation matrix connecting AVS and environmental screening metrics

Metric	BAA	$\hat{\eta}$	Spec. E	Mass	GHG	CED	Renew.
BAA	1.00	0.83	-0.57	-0.62	-0.27	-0.56	0.66
$\hat{\eta}$	0.83	1.00	-0.83	-0.82	-0.33	-0.72	0.71
Spec. E	-0.57	-0.83	1.00	0.96	0.68	0.95	-0.89
Mass	-0.62	-0.82	0.96	1.00	0.58	0.92	-0.94
GHG	-0.27	-0.33	0.68	0.58	1.00	0.84	-0.71
CED	-0.56	-0.72	0.95	0.92	0.84	1.00	-0.94
Renew.	0.66	0.71	-0.89	-0.94	-0.71	-0.94	1.00

The correlation matrix is descriptive, not causal. Within this virtual design space, BAA correlates positively with $\hat{\eta}$ (correlation coefficient 0.83) and renewable content (0.66), while mass is strongly associated with the specific-stiffness proxy (0.96) and CED (0.92). Because several quantities share common composition rules, these correlations should not be interpreted as experimentally independent relationships.

3.6. Engineering translation to automotive interior components

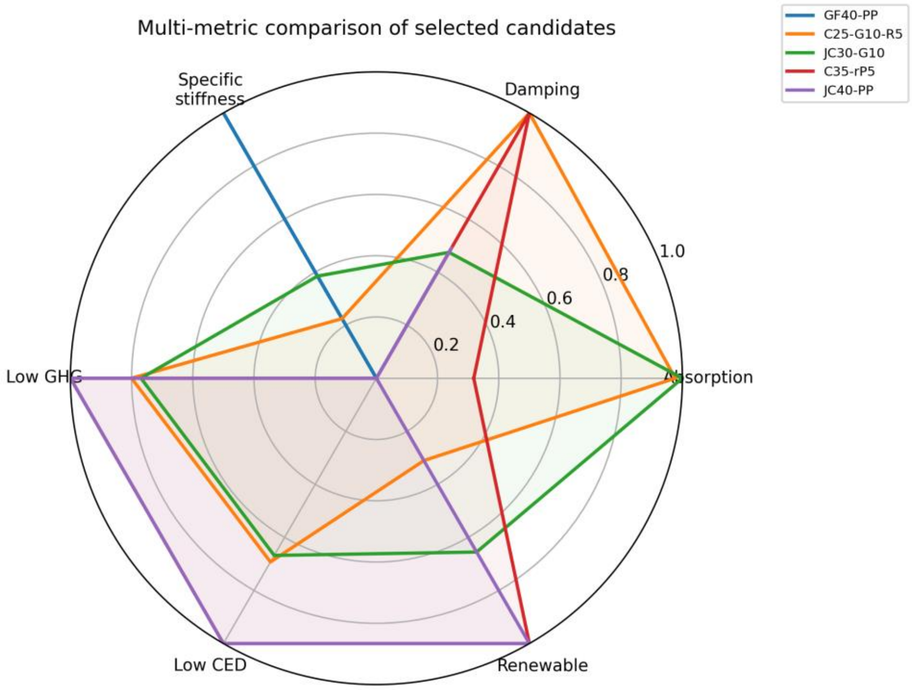

Fig. 7. Multi-criteria comparison of selected candidates; stiffness is a structural-response proxy, not a direct harshness measure

Table 10. Engineering translation of the screening results to automotive interior components

Automotive application	Preferred candidate	Technical rationale	Validation priority
Roof liner / headliner absorber	C35-rP5; JC40-PP reference	Low mass and low constituent-production burden; thickness remains the dominant modeled acoustic lever	Moisture uptake, sag stiffness and impedance-tube validation
Door inner trim acoustic pad	JC30-G10	Balanced top-three-stable profile with glass stiffness margin	Attachment pull-out, water exposure and acoustic validation
Dashboard hush panel	C25-G10-R5	Highest robust MCDA score under the disclosed damping scenario	Thermal aging, odor/VOC and measured damping
Floor tunnel / firewall secondary layer	C25-G10-R5	Damping-oriented proxy profile with moderate stiffness retention	Flammability, odor, temperature and mass
Carbon-minimizing nonstructural pad	C35-rP5	Lowest-carbon true-hybrid cluster and low areal mass	Moisture resistance and durability
High-impact local reinforcement	J20-A10-R5 only where essential	Aramid may serve localized functional needs but is environmentally unfavorable at full-area scale	Use only after impact testing and component-level necessity assessment

The radar chart intentionally uses specific stiffness rather than a direct harshness axis. Harshness is a perceptual response influenced by frequency content, structural transfer paths, mounting conditions and psychoacoustic context; none of these were modeled directly. Specific stiffness is included only because structural flexibility can affect vibration response and radiated noise near resonance. It is therefore an engineering structural-response proxy, not a measurement or prediction of perceived harshness.

No single material dominates every axis. C25-G10-R5 is favored by the disclosed damping scenario and robust MCDA weights, JC30-G10 offers a more conservative glass-containing balance, and C35-rP5 provides the strongest low-carbon/low-mass route. The correct component choice depends on measured acoustic response, mechanical requirements, moisture, flammability, VOC and attachment constraints.

3.7. Uncertainty, limitations and laboratory validation roadmap

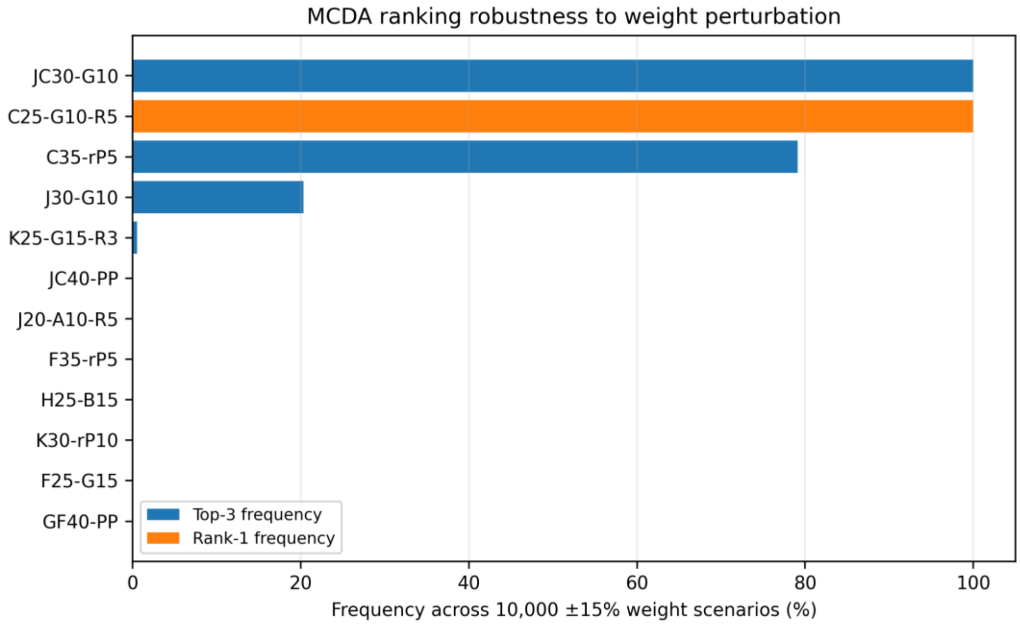

Fig. 8. Top-three frequency under 10,000 MCDA scenarios with all weights varied independently by +/-15%

The analysis separates three uncertainty classes. First, thickness is treated as an independent geometric factor in the primary comparison. Second, φ, σ, η̂ and architecture efficiencies are explicit screening assumptions; they are reproducible but unmeasured. Third, GHG factors and decision weights are treated probabilistically or through scenario perturbation. This separation makes clear which conclusions are model-dependent and which are robust within the stated uncertainty ranges.

Table 11. Validation roadmap for converting the screening framework into an experimentally validated study

Uncertainty source	Relative importance	Reason	Validation action
Thickness tolerance	High	Directly shifts modeled absorption and areal mass	Measure compressed thickness; test 16/20/24 mm systematically
Airflow resistivity σ	High	Primary Miki-model input	Measure airflow resistance/resistivity for every formulation
Open porosity φ	High	Controls density and porous-acoustic plausibility	Measure by gas pycnometry and/or validated imaging
Damping proxy coefficients	High	Current η̂ is assumption-driven	Measure loss factor and modulus using ASTM E756-type procedures
Model applicability	High	Miki assumes porous fibrous behavior	Compare predictions with measured impedance-tube spectra and consider Biot/JCAL models if needed
Moisture uptake	Medium-high	May change stiffness, mass and damping	Condition specimens at multiple RH levels
GHG/CED inventory factors	Medium	Sourcing and energy mix change results	Replace screening factors with traceable regional database inventory and full process energy
Fiber orientation and bonding	Medium	Affects effective modulus and damping	Use microscopy, tensile/flexural tests and DMA
Fire, odor and VOC behavior	Application-specific	Critical for automotive-cabin qualification	Perform OEM-relevant flammability and emissions testing

The principal limitation is the absence of measured specimens. The paper is therefore positioned as a transparent computational screening study. The next experimental phase should fabricate at least C25-G10-R5, JC30-G10 and C35-rP5 together with GF40-PP and JC40-PP controls, measure airflow resistivity and open porosity, test normal-incidence absorption according to ISO 10534-2:2023 or ASTM E1050-24, and measure damping according to ASTM E756-05(2023) [37−39].

Table 12. External sanity check linking model choices to measured literature and model scope

Literature anchor	Reported direction	Role in the present study
Hybrid jute/aloe-vera composites [25]	Measured vibration and acoustic responses vary with hybrid architecture	Supports treating acoustic and damping behavior as measurable, architecture-sensitive quantities rather than assumed outcomes
Coir vibration study [28]	Damping response changes with coir-fiber content	Supports the direction of the coir damping hypothesis, not the numerical proxy value
Rubber-hemp porous composites [30]	Thickness strongly affects absorption; composition changes porosity and airflow resistivity	Directly supports separating thickness from composition and reporting σ/φ
Jute/PP acoustic composites [31]	Impedance-tube measurements show composition-dependent acoustic response in a relevant thermoplastic system	Supports the application domain while underscoring the need for validation
Miki porous model [36]	Empirical equivalent-fluid formulation requires airflow resistivity and is intended for porous fibrous media	Supports the explicit-input approach and the stated applicability limitation

4. Conclusions

The primary composition comparison uses a common 20 mm geometry. Under this condition, BAA values occupy a narrow range of 0.612-0.636, demonstrating that broadband absorption is strongly influenced by thickness and must be separated from composition effects. Thickness remains a dominant modeled acoustic variable. For representative natural-fiber-rich candidates, increasing thickness from 16 to 24 mm raises BAA from approximately 0.55 to 0.69. Composition and geometry should therefore be optimized as separate factors. The acoustic model is reproducible because open porosity, airflow resistivity, Miki equations, damping coefficients, architecture factors and normalization rules are fully disclosed. Nevertheless, φ, σ and $\hat{\eta}$ remain unmeasured screening inputs or proxies and require laboratory validation. Under 20,000-trial GHG-factor uncertainty propagation, non-aramid hybrid candidates show median constituent-production reductions of approximately 26-56% relative to the 20 mm GF40-PP benchmark, whereas the aramid-containing design is environmentally unfavorable. These results are environmental screening, not a full ISO-compliant comparative LCA. C25-G10-R5 ranks first under the baseline MCDA and in 100% of 10,000 +/-15% weight-perturbation scenarios. JC30-G10 remains in the top three in 100% of scenarios and C35-rP5 in 79.1%. The ranking is robust within the tested weight range but remains conditional on the disclosed model assumptions. The framework should be used for hypothesis generation and experimental down-selection. Impedance-tube, airflow-resistivity, porosity, mechanical and damping tests are required before any candidate is claimed to have validated automotive NVH performance.

Data availability statement

All deterministic model outputs used in the analysis are reported in the manuscript tables. The explicit equations, coefficients and bounds required to reproduce the calculations are provided in the Methods section. No proprietary or human-subject data were used. The machine-readable calculation tables and script are available from the corresponding author upon reasonable request.

References

[1] Kumar R, Muthukrishnan M, Felix Sahayaraj A. Effect of hybridization on natural fiber reinforced polymer composite materials - A review. Polym Compos 2023;44:4459-79. https://doi.org/10.1002/pc.27489

[2] Kudva A, Mahesha GT, Pai KD. Physical, thermal, mechanical, sound absorption and vibration damping characteristics of natural fiber reinforced composites and hybrid fiber reinforced composites: A review. Cogent Eng 2022;9:2107770. https://doi.org/10.1080/23311916.2022.2107770?urlappend=%3Futm_source%3Dresearchgate.net%26utm_medium%3Darticle

[3] Kalusuraman G, Kumaran ST, Balamurugan K, Sivashanmugam N, Sivaprakasam P, Kurniawan R, et al. Vibration studies on fiber reinforced composites - A review. J Nat Fibers 2023;20:2157361. https://doi.org/10.1080/15440478.2022.2157361

[4] Savran M, Aydin L. Material selection for hybrid natural fiber laminated composites in vibration using a stochastic optimization method. In: Hybrid Natural Fiber Composites. Elsevier; 2021. p. 281-307. https://doi.org/10.1016/B978-0-12-819900-8.00011-8

[5] Suriani MJ, Ilyas RA, Zuhri MYM, Khalina A, Sultan MTH, Sapuan SM, et al. Critical review of natural fiber reinforced hybrid composites: Processing, properties, applications and cost. Polymers 2021;13:3514. https://doi.org/10.3390/polym13203514

[6] Mazarbhuiya RM, Veeman D. A comprehensive review on free vibrational analysis of natural fibers reinforced composite materials. J Reinf Plast Compos 2025;45. https://doi.org/10.1177/07316844251364331.

[7] Jeyaguru S, Thiagamani SMK, Siengchin S, Subramanian J, Ebrahimnezhad-Khaljiri H, Sanjay MR, et al. Effect of various weaving architectures on mechanical, vibration and acoustic behavior of Kevlar-hemp intra-ply hybrid composites. Compos Part A Appl Sci Manuf 2024;176:107845. https://doi.org/10.1016/j.compositesa.2023.107845

[8] Bakhori SNM, Hassan MZ, Bakhori NM, Jamaludin KR, Ramlie F, Md Daud MY, et al. Physical, mechanical and perforation resistance of natural-synthetic fiber interply laminate hybrid composites. Polymers 2022;14:1322. https://doi.org/10.3390/polym14071322

[9] Chandgude S, Salunkhe S. Mechanical behavior of natural fiber-based hybrid polymeric composites for automobile components: State of the art. Polym Compos 2021;42:2678-703. https://doi.org/10.1002/pc.26045

[10] Asyraf MRM, Yahya MY, Hassan SH, Ilyas RA, Sheng DDCV, Mas'ood NN, et al. Hybrid synthetic and natural fibres in honeycomb sandwich composites for structural applications: A brief review. J Nat Fibre Polym Compos 2023. https://www.researchgate.net/publication/372134074_Hybrid_Synthetic_and_Natural_Fibres_in_Honeycomb_Sandwich_Composite_Structures_for_Structural_Applications_A_Brief_Review

[11] Nurazzi NM, Asyraf MRM, Athiyah SM, Shazleen SS, Rafiqah SA, Harussani MM, et al. A review on mechanical performance of hybrid natural fiber polymer composites for structural applications. Polymers 2021;13:2170. https://doi.org/10.3390/polym13132170

[12] Uppalapati S, Jani SP, Balasundaram MCR, Palanisamy S, Jesure BR, Ramar K, et al. Optimization and thermo-mechanical characterization of hybrid natural-synthetic fiber polymer composites with organic fillers. J Eng Fibers Fabr 2026;21:15589250261441592. https://doi.org/10.1177/15589250261441591?urlappend=%3Futm_source%3Dresearchgate.net%26utm_medium%3Darticle

[13] Namakka M, Rahman MR, Bakri MKB, Karuppasamy BD, Ahmmad MS, James AA, et al. Advancements in acoustic properties of natural waste biocomposites: Current trends, applications, and future perspectives. Adv Compos Hybrid Mater 2025;8:386. https://doi.org/10.1007/s42114-025-01427-6

[14] Choudhary S, Haloi J, Sain MK, Saraswat P, Kumar V. Systematic literature review on thermal and acoustic characteristics of natural fibre polymer composites for automobile applications. Mater Today Proc 2023;118. https://doi.org/10.1016/j.matpr.2023.01.349

[15] Ayakdas O. The design and optimization of multiscale hybrid nanocomposite structures for vibration and buckling behavior. 2024. https://gcris.iyte.edu.tr/entities/publication/4674bba8-4ccd-4bf7-b57f-7fc67713a11b

[16] Adam HM, Bogale TM, Paramasivam V. Natural fiber composites under dynamic loading: A comprehensive review of mechanical performance and structural integrity. Eng Reports 2026;8:e70722. https://doi.org/10.1002/eng2.70722

[17] Neto J, Queiroz HFM, Aguiar RAA, Lima RDAA, Cavalcanti DKK, Banea MD. A review of recent advances in hybrid natural fiber reinforced polymer composites. J Renew Mater 2022;10:561. https://doi.org/10.32604/jrm.2022.017434

[18] Krishnasamy P, Pandian ACK, Rajamurugan G, Jayaraman T, Maniyambath A, Chandran KJ. Dynamic mechanical behavior of mono/synthetic-natural fiber composites - A review. Eng Res Express 2022;4:042001. https://doi.org/10.1088/2631-8695/ac9bcd

[19] Okur N, Yaradanakul MC. Development of hybrid layered structures based on natural fabric reinforced composites and warp knitted spacer fabric for acoustic applications. J Ind Text 2022;51:2216S-2245S. https://doi.org/10.1177/1528083721994677?urlappend=%3Futm_source%3Dresearchgate.net%26utm_medium%3Darticle

[20] Khan MKA, Mujahid Y, Alahmed N, Khan KA. A review of multifunctional hybrid fiber-reinforced polymer composites for aerospace applications. Adv Compos Hybrid Mater 2026;9. https://doi.org/10.1007/s42114-026-01626-9

[21] Kudva A, Mahesha GT, Hegde S, Pai D. Aging behavior of chemically treated bamboo/carbon fiber-reinforced hybrid composites: Evaluation of mechanical, acoustic, and vibrational properties. J Mater Res Technol 2025;38: 2220−30. https://doi.org/10.1016/j.jmrt.2025.08.057

[22] Bisheh H. Natural frequencies for bending vibrations of smart laminated composite plates reinforced with bamboo fibres. Smart Mater Methods 2024;1:351−74. https://doi.org/10.1080/29963176.2024.2421868

[23] Salve A, Mache A, Munde YS, Jain S. Dynamic and damping characteristics of jute-glass hybrid polymer composites reinforced with metallic wire mesh. J Vib Eng Technol 2025;13:522. https://doi.org/10.1007/s42417-025-02098-9

[24] Turyahabwe A, Dennison MS, George OS. Hybrid natural fiber composites for automotive interior applications: A comprehensive review. I-Manager's J Mater Sci 2025;13. https://doi.org/10.26634/jms.13.2.22313

[25] Senthilrajan S, Venkateshwaran N, Giri R, Ismail SO, Nagarajan R, Krishnan K, Mohammad F. Mechanical, vibration damping and acoustics characteristics of hybrid aloe vera/jute/polyester composites. J Mater Res Technol 2024;31:2402−13. https://doi.org/10.1016/j.jmrt.2024.06.158.

[26] Temesgen AG. A research on the use of enset woven fabric structures for the applications of sound absorption and biodegradable composite material development. Bursa Uludağ Üniversitesi 2021. https://acikerisim.uludag.edu.tr/entities/publication/95bca94e-c61e-44a0-bc40-e7db33def995

[27] Nakhaeipour M, Forouharmajd F, Habibi E, Soltani P, Tehrani A. Acoustic performance optimization of natural-fiber micro-perforated panels backed by an optimized polyurethane-fibrogranule composite. Sci Rep 2026;16. https://doi.org/10.1038/s41598-026-35058-8

[28] Nikhil KV, Ramasubramanian S, Gudimetla A, Amarnath G, Sathishkumar G, Pugazhenthi R, et al. Experimental investigation on vibration characteristics and damping performance of coir fiber-reinforced polymer composites material. Discov Appl Sci 2025;7:465. https://doi.org/10.1007/s42452-025-07013-1.

[29] Tengku MIS, Marsi N, Hassan NNM, Hassan AM, Leman AM, Abidin AMZ, et al. Dynamic stiffness and damping behaviour of chemically treated PEFB-fiberglass hybrid composites for insulation applications. J Phys Conf Ser 2025;3156:012012. https://doi.org/10.1088/1742-6596/3156/1/012012

[30] Astrauskas T, Balčiūnas G, Bradulienė J, Ružickij R, Naimušin A, Januševičius T. Acoustic and thermal insulation properties of rubber-hemp shive composite bonded with regenerated polyurethane resin. Sci Rep 2026;16:4851. https://doi.org/10.1038/s41598-026-35411-x.

[31] Shen J, Li K, Yan J. Mechanical and acoustic properties of jute fiber-reinforced polypropylene composites. ACS Omega 2021;6:31154−60. https://doi.org/10.1021/acsomega.1c04605.

[32] Pingulkar H, Mache A, Munde Y, Siva I. Synergy of interlaminar glass fiber hybridization on mechanical and dynamic characteristics of jute and flax fabric reinforced epoxy composites. J Nat Fibers 2022;19:4310−25. https://doi.org/10.1080/15440478.2020.1856280

[33] Liu Z, Dong C, Tong L, Rudd C, Liu X, Yi X. A pre-screening study of honeycomb sandwich structure filled with green materials for noise reduction. Compos Part A Appl Sci Manuf 2022;163:107226. https://doi.org/10.1016/j.compositesa.2022.107226

[34] Wang B, Huang S, Yan L. Natural/synthetic fiber-reinforced bioepoxy composites. In: Bio-Based Epoxy Polymers, Blends, and Composites. 2021. p. 73−116. https://doi.org/10.1002/9783527823604.ch2

[35] Altaee MA, Mostafa NH. Mechanical properties of interply and intraply hybrid laminates based on jute-glass/epoxy composites. J Eng Appl Sci 2023;70:121. https://doi.org/10.1186/s44147-023-00293-7

[36] Miki Y. Acoustical properties of porous materials - Modifications of Delany-Bazley models. J Acoust Soc Jpn (E) 1990;11:19-24. https://doi.org/10.1250/AST.11.19
[37] International Organization for Standardization. ISO 10534-2:2023. Acoustics - Determination of acoustic properties in impedance tubes - Part 2: Two-microphone technique for normal sound absorption coefficient and normal surface impedance. Geneva: ISO; 2023. https://www.iso.org/standard/81294.html
[38] ASTM International. ASTM E1050-24. Standard Test Method for Impedance and Absorption of Acoustical Materials Using a Tube, Two Microphones and a Digital Frequency Analysis System. West Conshohocken, PA: ASTM International; 2024. https://store.astm.org/e1050-24.html
[39] ASTM International. ASTM E756-05(2023). Standard Test Method for Measuring Vibration-Damping Properties of Materials. West Conshohocken, PA: ASTM International; 2023. https://store.astm.org/e0756-05r17.html
[40] Glass Fibre Europe. Life Cycle Assessment of Continuous Filament Glass Fibre Products. Brussels: Glass Fibre Europe; 2023. https://glassfibreeurope.eu/wp-content/uploads/2023/02/GFE_LCA-report-2023-February-2023.pdf
[41] American Chemistry Council. Cradle-to-Gate Life Cycle Analysis of Polypropylene (PP) Resin. Washington, DC: ACC Plastics Division; 2021. https://www.americanchemistry.com/better-policy-regulation/plastics/resources/cradle-to-gate-life-cycle-analysis-of-polypropylene-pp-resin
[42] The Association of Plastic Recyclers. Virgin vs. Recycled Plastic Life Cycle Assessment Energy Profile and Life Cycle Assessment Environmental Burdens. Report prepared for the Association of Plastic Recyclers; 2020. https://plasticsrecycling.org/wp-content/uploads/2024/08/APR-Recycled-vs-Virgin-LCA-May2020.pdf
[43] Deng Y, Tian Y. Assessing the environmental impact of flax fibre reinforced polymer composites from a consequential life cycle assessment perspective. Sustainability 2015;7:11462–83. https://doi.org/10.3390/su70911462.